Optical and magneto-optical polar Kerr spectra of Fe_3O_4 and Mg^{2+}- or Al^{3+}-substituted Fe_3O_4

W. F. J. Fontijn and P. J. van der Zaag*

Philips Research Laboratories, Prof. Holstlaan 4, 5656 AA Eindhoven, The Netherlands

M. A. C. Devillers

Research Institute for Materials, High Field Magnet Laboratory, P.O. Box 9010, 6500 GL Nijmegen, The Netherlands

V. A. M. Brabers

Department of Solid State Physics, Eindhoven University of Technology, P.O. Box 513, 5600 MB Eindhoven, The Netherlands

R. Metselaar

Department of Solid State Chemistry and Materials Science, Eindhoven University of Technology, P.O. Box 513, 5600 MB Eindhoven, The Netherlands

The diagonal elements of the dielectric tensor, between 0.5 and 5.0 eV, and the magneto-optical polar Kerr spectra, between 0.7 and 4.0 eV, have been determined for a synthetic crystal of magnetite, Fe_3O_4 and a systematic investigation of these properties for Mg^{2+} and Al^{3+} substitutions has been carried out. From these spectra the off-diagonal elements of the dielectric tensor was calculated between 0.7 and 4.0 eV. Through fitting simultaneously both the diagonal and the off-diagonal elements of this tensor with one set of parameters and consistently for all partially substituted ferrite samples, we were able to resolve the magneto-optical spectrum of Fe_3O_4 between 0.7 and 4.0 eV. The observed trends in the major transitions upon substitution provide the experimental evidence for intervalence charge transfer and intersublattice charge transfer transitions in Fe_3O_4. [S0163-1829(97)03833-2]

I. INTRODUCTION

Magnetite crystallizes in the inverse spinel structure, with cation distribution $(Fe^{3+})[Fe^{3+}Fe^{2+}]O_4$. In this structural formula the parentheses denote tetrahedral (A) sites and the square brackets denote the octahedral (B) sites. For most purposes, Fe_3O_4 can be considered to be the prototype of an inverse spinel ferrite. Most of the properties of ferrites have been thoroughly studied and are well documented.[1,2] However, the electronic structure of Fe_3O_4, as well as that of other transition-metal (TM) oxides such as NiO, is still a subject of debate.[3–9] In transition-metal oxides the valence bands of oxygen $2p$ character are separated from the transition-metal ion's empty $4s$ band by an energy gap of several (4–6) eV.[3,5] The TM $3d$ electrons are considered to interact strongly with the surrounding oxygen anions to form more or less localized states. These states are spread out over a wide energy range, because of the strong Coulomb repulsion between d electrons. This repulsion splits the d^n configuration into various multiplets, which are further split by the crystal field. As a consequence $3d$-derived bands appear usually both within and above the O $2p$ TM $4s$ gap. For the particular case of Fe_3O_4 the actual conductivity gap, i.e., the valence band to conduction band gap, is assumed to be of $3d \leftrightarrow 3d$ nature,[8] but clearly a variety of other neutral excitations exists. Understandably, this rather complex electronic structure of TM oxides has led for Fe_3O_4 and related ferrites to a confusing variety of interpretations of the optical and magneto-optical (MO) Kerr spectra, due to different assignments of the observed transitions.

Various studies on the magneto-optical properties of mag-

netite and substituted spinel ferrites in the visible and near infrared part of the spectrum have been reported in the past. Šimša and co-workers reported the polar Kerr rotation and ellipticity of Fe_3O_4 as well as the influence of a systematic substitution of Fe^{2+} by Mn^{2+} in the 0.5–3.0 eV energy range.[10,11] In their study the peak at 0.9 eV in the Kerr rotation spectrum of Fe_3O_4 was ascribed to the presence of charge carriers (i.e., Fe^{2+}) and was assumed to be related to charge transfer between $[Fe^{2+}]$ and $[Fe^{3+}]$. The spectrum around 2.0 eV was explained in terms of $3d$ crystal-field transitions of iron ions on tetrahedral sites. Zhang and co-workers also reported the polar Kerr spectra and the off-diagonal element of the dielectric tensor of Fe_3O_4 between 0.5 and 4.3 eV,[12] and in addition that of $Li_{0.5}Fe_{2.5}O_4$ and $MgFe_2O_4$ between 0.5 and 5.0 eV.[13] All major peaks in the Kerr spectrum of Fe_3O_4 were assigned to $3d^n \rightarrow 3d^{n-1} 4s$ orbital promotion processes. Also Višňovský *et al.* reported polar Kerr spectra of $Li_{0.5}Fe_{2.5}O_4$ and $MgFe_2O_4$, and derived the complete dielectric tensor of the latter compound between 2.0 and 6.0 eV.[14] Bands at 3.4, 3.6, 4.3, and 4.7 eV were identified as $2p \rightarrow 3d$ charge-transfer transitions between O^{2-} and Fe^{3+}. Finally, Peeters and Martens reported the polar Kerr rotation of $CoFe_2O_4$ between 0.6 and 5.5 eV.[15] Bands below 3.0 eV were assigned to crystal-field transitions of Co^{2+}, and around 2.0 eV a charge-transfer transition between $[Co^{2+}]$ and $[Fe^{2+}]$ was identified. Thus, despite considerable experimental efforts, no coherent picture concerning the microscopic origin of the MO active transitions in Fe_3O_4 and related substituted spinel ferrites is available. For the sake of completeness, we should mention a possible Drude term or, in other words, the intraband transitions (see,

for instance, the analysis of Ga by Erskine and Stern[16]). In Fe_3O_4 these transitions occur around 0.2 eV,[17] and therefore do not play a role in the energy range investigated here.

The problem with the interpretations given so far is that Fe_3O_4 exhibits a relatively strong MO-Kerr effect in the visible region and absorption peaks with an oscillator strength, f, of about 10^{-3}.[7] The interpretations given above are based on transitions which are either spin or parity forbidden, and in some cases even both. For instance, crystal-field transitions involving Fe^{3+} are spin forbidden, while in addition crystal-field transitions on octahedral sites are parity forbidden. On the tetrahedral site, crystal-field transitions are not strictly parity forbidden due to the lack of inversion symmetry in the crystal field at that site. As a result the oscillator strength of crystal-field transitions is expected to be about 10^{-4}–10^{-5}.[18] In a similar way orbital promotion processes $d \rightarrow s$ via an electric dipole transition are forbidden since $\Delta l = 2$. Moreover, $d \rightarrow s$ transitions involving iron ions on a centrosymmetric, octahedral site are parity forbidden. Only due to distortion of the octahedral symmetry may the parity selection rule be weakened.[13] Therefore, the most recent theoretical work on the Kerr spectrum of Fe_3O_4 by Feil suggests that the main transitions in the region between 0.5 and 3 eV are intervalence charge transfer (IVCT) transitions,[7] while the transitions between 3 and 4 eV are both IVCT transitions and intersublattice charge transfer (ISCT) transitions as proposed for $Y_3Fe_5O_{12}$ by Scott.[18] In an IVCT transition between $[Fe^{2+}]$ and $[Fe^{3+}]$ the total spin of the ion pair is unchanged. Furthermore, such a $[Fe^{2+}]$-$[Fe^{3+}]$ pair does not possess inversion symmetry, and consequently the parity selection rule is relaxed.[18] Therefore, one would expect IVCT transitions to have a much higher oscillator strength than crystal-field and orbital promotion transitions. And as a result, if occurring in Fe_3O_4, one would expect IVCT transitions to dominate the spectrum. In this paper, we present a systematic study of the influence on the MO-Kerr spectrum and the dielectric tensor of Fe_3O_4, of partial substitution of $[Fe^{2+}]$ by Mg^{2+} and of $[Fe^{3+}]$ by Al^{3+}, with the concentration of the substituent as a parameter. These substituents have the advantage over those used in previous studies[11,15] that Mg^{2+} and Al^{3+} are nonmagnetic ions which therefore do not contribute directly to the MO spectrum, in contrast to Co^{2+} and Mn^{2+}. Moreover, because of the variable degree of substitution, trends in MO-peak intensity and energy shift can be established. Furthermore, Mg^{2+} and Al^{3+} both preferentially occupy only one site: the octahedral site.[19,20] As a result we are able to establish firmly the nature of the MO-active transitions. In the calculated off-diagonal tensor element of the substituted samples we find clear evidence for the IVCT transitions.

The organization of this paper is as follows: In Sec. II we discuss the theoretical background, i.e., the Kerr effect, the dielectric tensor, and intervalence charge transfer transitions. Section III deals with the experimental procedures. Subsequently, in Sec. IV, the experimental results are presented, i.e., the complete dielectric tensor and the Kerr spectra of pure Fe_3O_4 and substituted Fe_3O_4. Then, in Sec. V, the data are analyzed and discussed. Finally our conclusions are given in Sec. VI.

II. THEORETICAL BACKGROUND

A. Macroscopic theory: The Kerr effect

The MO-Kerr effect is caused by electronic transitions in a magnetic material, of which the degeneracy of the orbital quantum number m_l is lifted, due to spin-orbit coupling. This gives rise to optical anisotropy; the off-diagonal element of the dielectric tensor will be nonzero.

The polar Kerr effect is the change in the polarization state of a light beam which is reflected at normal incidence on a perpendicularly magnetized sample. The Kerr rotation θ_k is related to the change in the phase in the polarization state of the light reflected from the surface and the Kerr ellipticity ϵ_k to the change in amplitude. To a first approximation the Kerr effect depends linearly on the magnetization. The Kerr effect signal originates from a surface layer of which the thickness is approximately twice the penetration depth of the light, d_p. This is defined as the depth for which the intensity of the light is reduced by a factor e^{-1}: $d_p = \lambda/(4\pi k)$ where k is the absorption coefficient and λ the wavelength.

The dielectric tensor for a crystal with cubic symmetry magnetized in the z direction (perpendicular to the surface) has in the convention used in this paper the form

$$\tilde{\varepsilon} = \begin{vmatrix} \widetilde{\varepsilon}_{xx} & \widetilde{\varepsilon}_{xy} & 0 \\ -\widetilde{\varepsilon}_{xy} & \widetilde{\varepsilon}_{xx} & 0 \\ 0 & 0 & \widetilde{\varepsilon}_{zz} \end{vmatrix}, \quad (1)$$

with $\widetilde{\varepsilon}_{xx} = \varepsilon'_{xx} + i\varepsilon''_{xx}$; $\widetilde{\varepsilon}_{xy} = \varepsilon'_{xy} + i\varepsilon''_{xy}$.

The relation of the elements of this tensor to the refractive index n, the absorption coefficient k, and the Kerr rotation θ_k and ellipticity ϵ_k, is for the polar Kerr effect given by[21]

$$\varepsilon'_{xx} = n^2 - k^2; \quad \varepsilon''_{xx} = 2nk,$$

$$\varepsilon'_{xy} = A\theta_k - B\epsilon_k,$$

$$\varepsilon''_{xy} = -B\theta_k - A\epsilon_k, \quad (2)$$

with $A = (n^3 - 3nk^2 - n)$; $B = (-k^3 + 3n^2k - k)$.

B. Microscopic theory: The dielectric tensor

At a microscopic level the diagonal element of the dielectric tensor is for single-ion electric-dipole transitions given by[22]

$$\widetilde{\varepsilon}_{xx} = 1 + \sum_{e,u} \widetilde{\varepsilon}_{xx,e(u)}$$

$$= 1 + \frac{4\pi Ne^2}{m}$$

$$\times \sum_{e,u} f_{e,u} \left[\frac{\omega_{e(u)}^2 - \omega^2 + \Gamma_{e(u)}^2 - 2i\omega\Gamma_{e(u)}}{(\omega_{e,(u)}^2 - \omega^2 + \Gamma_{e(u)}^2)^2 + 4\omega^2\Gamma_{e(u)}^2} \right], \quad (3)$$

where N is the number of active absorbing centers per unit volume, e the electronic charge, and m the electronic mass. Further, $\omega_{e(u)}$ and $\Gamma_{e(u)}$ are the resonance frequency and half-width at half-maximum of the optical transitions between the ground state $|g\rangle$ and excited states $|e(u)\rangle$ with u indicating the orbital degeneracy. If $\Gamma_{e(u)}/\omega_{e(u)} \leqslant 1$ applies

the maximum of ϵ''_{xx} occurs at $\omega=\omega_{e(u)}$ and the oscillator strength, $f_{e,u}$, is given to a good approximation by[22]

$$f_{e,(u)}=\frac{m}{2\pi Ne^2 L}\,\omega_{e(u)}\Gamma_{e(u)}(\varepsilon''_{xx,e(u)})_{\max},\qquad(4)$$

where L is the Lorentz local field correction, $L=[(n^2+2)^2/9]$, which must be applied since for Fe_3O_4 the condition that $|\varepsilon''_{xx}-1|\ll 1$ does not hold.[23] For electric dipole transitions the off-diagonal element is given by[22]

$$\widetilde{\varepsilon}_{xy}=\sum_{e,u}\widetilde{\varepsilon}_{xy,e(u)}$$

$$=\frac{2\pi Ne^2}{m}\sum_{e,u}\left[\frac{f_{-e(u)}-f_{+e(u)}}{\omega^2-\omega^2_{e,(u)}-\Gamma^2_{e(u)}-2i\omega\Gamma_{e(u)}}\right]$$

$$\times\frac{\omega-i\Gamma_{e(u)}}{\omega_{e,(u)}},\qquad(5)$$

where $f_{\pm e(u)}$ are the oscillator strengths for transitions caused by right and left circularly polarized light (RCP and LCP, respectively).

The optical anisotropy in materials which exhibit a Kerr effect arises from spin-orbit coupling. Due to the spin-orbit coupling the electron system is able to distinguish between LCP and RCP. In our investigation two special cases are relevant which result in two distinct types of line shapes.

In the first case the contribution to $\widetilde{\varepsilon}_{xy}$ is dominated by the energy splitting $\Delta\omega$ between excited states $|e(-)\rangle$ and $|e(+)\rangle$, for instance, a transition between an orbital singlet ground state and a spin-orbit split excited state. In this case an energy splitting between the transition energies for RCP and LCP arises, while $f_{+e(u)}=f_{-e(u)}$. A so-called type-I line shape is observed: an extremum in ε'_{xy} and an oscillation in ε''_{xy}, corresponding to dissipative and dispersive behavior, respectively. This is historically called a diamagnetic line shape. Examples are spin-allowed charge transfer bands. In this case the following equation describes the transition:

$$\widetilde{\varepsilon}_{xy}=-\Gamma^2_0(\varepsilon'_{xy})_{\max}\frac{(\omega-\omega_0)^2-\Gamma^2_0+2i\Gamma_0(\omega-\omega_0)}{[(\omega-\omega_0)^2+\Gamma^2_0]^2},\quad(6)$$

where ω_0 and Γ_0 are the resonance frequency and half-width at half-maximum for the particular transition.

In the second case, the contribution to $\widetilde{\varepsilon}_{xy}$ is dominated by a difference between $f_{+e(u)}$ and $f_{-e(u)}$ as can be caused by a difference in ground-state population of the levels of a spin-orbit split ground state, for example, a transition between an orbitally degenerate ground state and an orbital singlet excited state. In this case the oscillator strengths $f_{+e(u)}$ and $f_{+e(u)}$ for RCP and LCP light differ and an type-II line shape is observed: an oscillation in ε'_{xy} and an extremum in ε''_{xy}. This is a so-called paramagnetic line shape. For instance, the spin- and parity-forbidden crystal-field transitions show such a behavior. For this type of transition the following expression applies:

$$\widetilde{\varepsilon}_{xy}=-2\Gamma_0(\varepsilon''_{xy})_{\max}\frac{\omega(\omega^2-\omega^2_0+\Gamma^2_0)-i\Gamma_0(\omega^2+\omega^2_0-\Gamma^2_0)}{(\omega^2-\omega^2_0-\Gamma^2_0)^2+4\Gamma^2_0\omega^2}.\qquad(7)$$

More details can be found in Refs. 22–24.

C. Intervalence charge transfer

Intervalence charge transfer (IVCT) transitions are transitions in which an electron, through optical excitation, is transferred to a neighboring cation. Mixed valence compounds, i.e., compounds containing an element in two different oxidation states, such as Fe in Fe_3O_4, often show unusually intense absorption in the visible region that can be attributed to IVCT transitions.[25,26] Overlapping $Fe(3d)$ orbitals, across the shared edges of adjacent Fe-O polyhedra, result in weak Fe-Fe bonds. The IVCT bands are the result of electronic transitions between the Fe-Fe bonding and antibonding orbitals. In Fe_3O_4 the electron transfer between Fe^{2+} and Fe^{3+} may be mediated by O^{2-} ions, in particular when e_g orbitals are involved. In such a case, the transfer occurs more readily for smaller electrostatic polarization of the O^{2-} ions.[25,27] Between Fe t_{2g} orbitals direct electron transfer is possible as a result of the overlap between these orbitals.

The intensity and transition energy of an IVCT are sensitive to changes in the lattice. Factors to be considered are equivalence of sites, the distance between the sites x and y, R_{xy}, and the degree of delocalization of the electron involved, α. Using the standard optical matrix element one can derive the following expression for the oscillator strength, f, of IVCT transitions:[7,27]

$$f=1.085\times10^{-5}\nu\alpha^2(1-\alpha^2)R^2_{xy}\qquad(8)$$

with ν the wave number at which the transition occurs. Combining Eq. (8) and Eq. (4), and neglecting effects on R_{xy} and ν, yields

$$(\varepsilon_{xy})_{\max}\propto N\alpha^2(1-\alpha^2)\qquad(9)$$

with N the number of absorbing species per unit volume. We thus find that $(\varepsilon_{xy})_{\max}$ depends in a nonlinear way on the degree of delocalization, α. For a given IVCT a change in the lattice which diminishes the equivalence of sites or increases the distance between the cations will increase the localization of the electron, increasing the transition energy and lowering oscillator strength. Examples are increased polarization of the intermediate oxygen and localized distortions due to vacancies or substitutions. We refer to the literature for more general discussions on IVCT transitions[25,26] as well as more quantitative ones.[7,27–29]

Finally, it should be noted that the so-called intersublattice charge transfer transitions described by Scott and co-workers[18,24] are IVCT transitions between Fe^{3+} ions on different crystallographic sites.[23] For reasons of clarity we will still refer to these transitions as ISCT transitions in this paper.

III. EXPERIMENTAL PROCEDURES

The polar Kerr spectra from 0.7 to 4.0 eV (1700–310 nm), were measured for a series of single-crystalline spinel ferrite samples ([110] oriented) with varying degrees of Mg^{2+} or Al^{3+} substitution. A list of the samples studied is given in Table I. To prepare these samples, stoichiometric ($M_x Fe_{3-x}O_{4\pm0.002}$ with $M=Mg,Al$) polycrystalline rods

TABLE I. Survey of the single-crystalline spinel ferrite samples studied and the figures in which their spectra are presented.

Composition	Indication in figures and text	Figures
$Fe_2^{3+}Fe^{2+}O_4$	Fe_3O_4	1,2,4,5,7,8,11
$Mg_{0.1}^{2+}Fe_2^{3+}Fe_{0.9}^{2+}O_4$	0.1 Mg	11
$Mg_{0.2}^{2+}Fe_2^{3+}Fe_{0.8}^{2+}O_4$	0.2 Mg	2,5,8,11
$Mg_{0.4}^{2+}Fe_2^{3+}Fe_{0.6}^{2+}O_4$	0.4 Mg	11
$Mg_{0.8}^{2+}Fe_2^{3+}Fe_{0.2}^{2+}O_4$	0.8 Mg	2,5,8,11
$Al_{0.005}^{3+}Fe_{2.995}^{3+}Fe^{2+}O_4$	0.005 Al	
$Al_{0.02}^{3+}Fe_{2.98}^{3+}Fe^{2+}O_4$	0.02 Al	3,6,9,11
$Al_{0.2}^{3+}Fe_{2.8}^{3+}Fe^{2+}O_4$	0.2 Al	3,6,9,11
$Al_{0.4}^{3+}Fe_{2.6}^{3+}Fe^{2+}O_4$	0.4 Al	3,6,9,11

were prepared by ceramic techniques and subsequently recrystallized with a floating zone technique in nitrogen atmosphere ($P_{O_2} \approx 0.1$ Pa). The obtained crystals were annealed at equilibrium oxygen pressure in the temperature range between 1200 and 1300 °C and cooled slowly in 3 h to room temperature in an adjusted atmosphere to prevent oxidation. In addition, the Mg-substituted crystals were wrapped into Pt foils and further annealed in evacuated and sealed silica tubes for 4 h at 600 °C, followed by slowly cooling with 12 °C/h to room temperature. This procedure yields high-quality stoichiometric single crystals and due to the slow cooling rate more than 95% of the Mg^{2+} and Al^{3+} substituents will be located at octahedral sites as well as 100% of the Fe^{2+}.[19,20] Thus, these ferrites have a well-defined cation distribution whereas ferrites prepared through other methods may have a more random, nonequilibrium cation distribution.[30] A detailed description of the preparation techniques employed can be found elsewhere.[31] For the magneto-optical measurements platelets were cut from the crystals and Syton polished to mirror finish.

For the Kerr measurements the following setup was used: Light from a 450 W Xe arc lamp (Osram XBO) is focused with a set of mirrors on the entrance slit of a monochromator (SPEX 1702). The beam from the monochromator passes a filter, a Glan-Thompson polarizer, a photoelastic modulator (Hinds CF5), and a lens which focuses the light on the sample, situated between the poles of a 1400 kA/m water-cooled electromagnet. After reflection from the sample, the light passes through a lens, a chopper, and an analyzer before reaching the detector. This is either a Ge photodiode (Rofin 7460) for the 0.7–1.4 eV range or a photomultiplier (Hamamatsu R943-02) for the 1.4–4.0 eV range. The detector signal was preamplified (current to voltage) and fed into three lock-in amplifiers (EG&G 5209, 5205, and 5207) to measure the light intensity, rotation and ellipticity. The setup was controlled by a Hewlett Packard computer (HP-300). This setup is similar to the one described by Martens et al.[32] A detailed description of the employed measuring technique using a photoelastic modulator (PEM) has been given by Sato.[33]

Kerr rotation and ellipticity, θ_k and ϵ_k, were measured at ambient temperature, with a saturating magnetic field applied perpendicularly to the sample surface (1400 kA/m). By averaging measurements in opposite field directions any offset

in Kerr amplitude due to the setup is eliminated. More details on the Kerr spectrometer and measurement procedure can be found elsewhere.[34] The diagonal element of the dielectric tensor between 0.5 and 5.0 eV was obtained through spectroscopic ellipsometry as described previously.[35]

IV. EXPERIMENTAL RESULTS

A. Absorption spectra

In Figs. 1–3 the diagonal element of the dielectric tensor of Fe_3O_4 and several Mg^{2+}- or Al^{3+}-substituted samples are shown. These spectra were obtained from spectroscopic ellipsometry measurements and were subsequently used in the calculation of the off-diagonal element of the dielectric tensor from the Kerr measurements by means of Eq. (2). Apart from the influence of substitution of $[Fe^{3+}]$ by Al^{3+} on ε_{xx}'' [Fig. 3(b)], which shows a nearly linear decrease in intensity with Al^{3+} concentration over the entire spectral range investigated, no clear trends are apparent in these spectra. This is due to the fact that ε_{xx} is composed of a large number of overlapping optical transitions, each possibly having a different dependence on, as well as energy shift with, the substituent concentration. Therefore, inspection of the ε_{xx} spectrum is insufficient to establish peak positions or trends in peak position or intensity. The complete dielectric tensor should be determined and all elements of this tensor should be fitted simultaneously with one set of parameters.

B. MO spectra

In Figs. 4–6 the Kerr spectra of Fe_3O_4 and of several of the Mg^{2+}- or Al^{3+}-substituted ferrites are presented. Both the measured polar Kerr spectrum (Fig. 4) and the derived off-diagonal element of the dielectric tensor (Fig. 7) of pure Fe_3O_4 are in fair agreement with those reported in the literature.[10,12,36] The best way to study magneto-optical transitions is to examine the off-diagonal element of the dielectric tensor, where diamagnetic and paramagnetic transitions can be identified at their exact frequency and linked to their microscopic origin. Therefore, we will focus on the dielectric
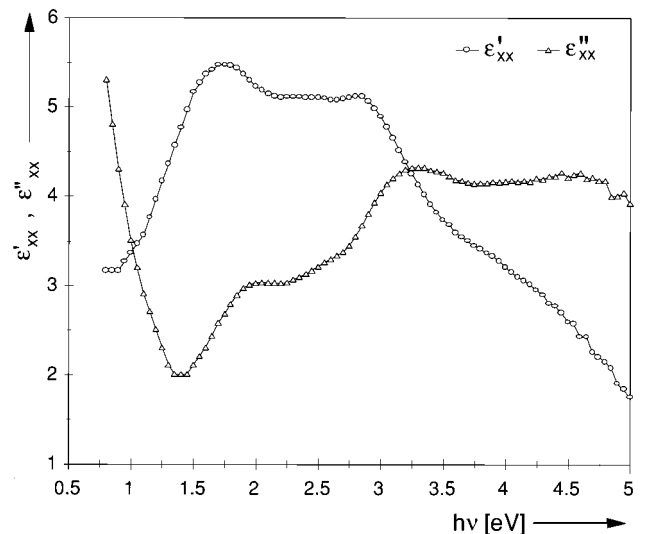
FIG. 1. The real (ε_{xx}') and imaginary (ε_{xx}'') part of the diagonal element of the dielectric tensor of Fe_3O_4.
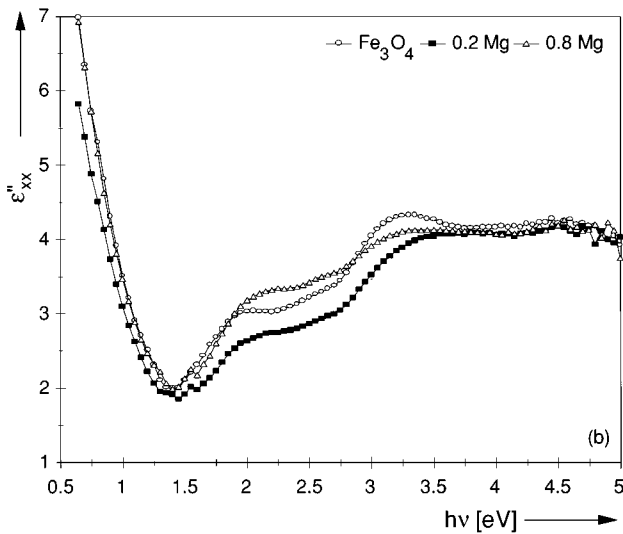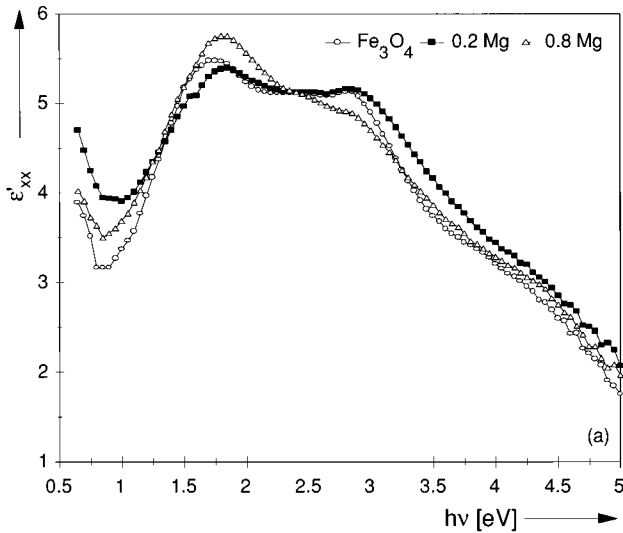
FIG. 2. The diagonal element of the dielectric tensor of $(Fe^{3+})[Mg_x^{2+}Fe_{(1-x)}^{2+}Fe^{3+}]O_4$ for $x = 0.0$, 0.2, and 0.8; (a) real part, ε'_{xx}; (b) imaginary part, ε''_{xx}.

FIG. 3. The diagonal element of the dielectric tensor of $(Fe^{3+})[Al_x^{3+}Fe^{2+}Fe_{(1-x)}^{3+}]O_4$ for $x = 0.02$, 0.2, and 0.4; (a) real part, ε'_{xx}; (b) imaginary part, ε''_{xx}.

tensor in the remainder of this paper. From Fig. 7 three major bands in the off-diagonal tensor element of pure magnetite are found: around 0.56 eV a paramagnetic band (only tail visible), around 1.94 eV a paramagnetic band, and around 3.0–4.0 eV a diamagnetic band. This last, broad shape is found to be composed of transitions at 3.11, 3.45, and 3.94 eV, as will be explained below.

Figure 8 shows the influence of Mg^{2+} substitution on the off-diagonal element of the dielectric tensor. Mg^{2+} mainly occupies B sites replacing $[Fe^{2+}]$. From Fig. 8 one can see that the transitions at 0.56 and 1.94 eV exhibit a nonlinear dependence on the Mg^{2+} content. The influence of substitution of Fe^{2+} with Mg^{2+} on the spectra in the 3.0–4.0 eV range is complex and requires a more detailed analysis given in the next section. Comparison of the position of the extrema for Fe_3O_4 and $Mg_{0.2}Fe_{2.8}O_4$, shows no shifts. This is consistent with the small effect Mg^{2+} substitution has on the lattice, since the lattice parameter of $MgFe_2O_4$ is only 0.3% smaller than that of Fe_3O_4, i.e., 8.370–8.380 Å versus 8.396 Å.[19,31]
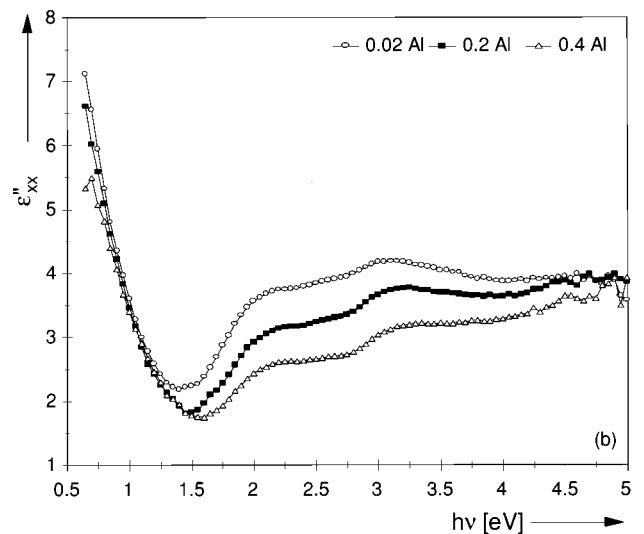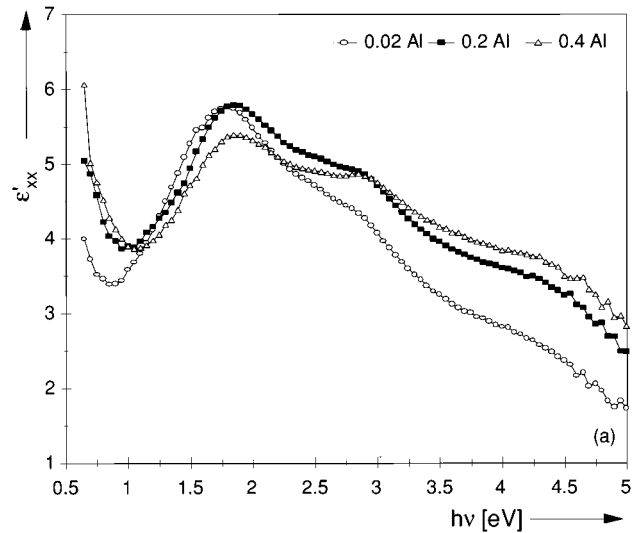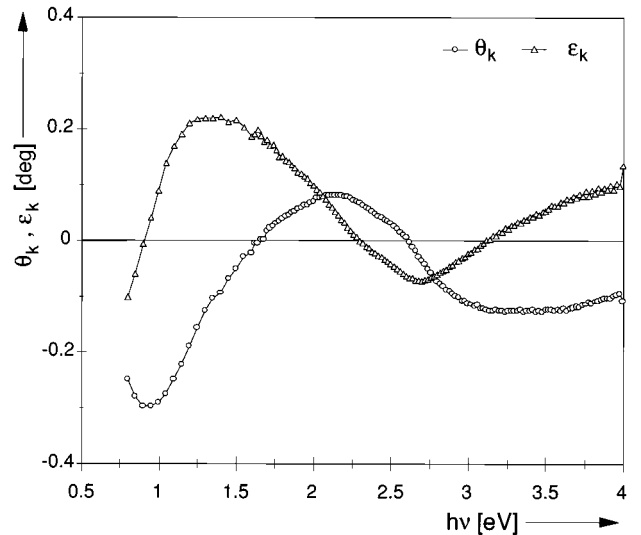
FIG. 4. The Kerr rotation θ_k and Kerr ellipticity ϵ_k of Fe_3O_4.
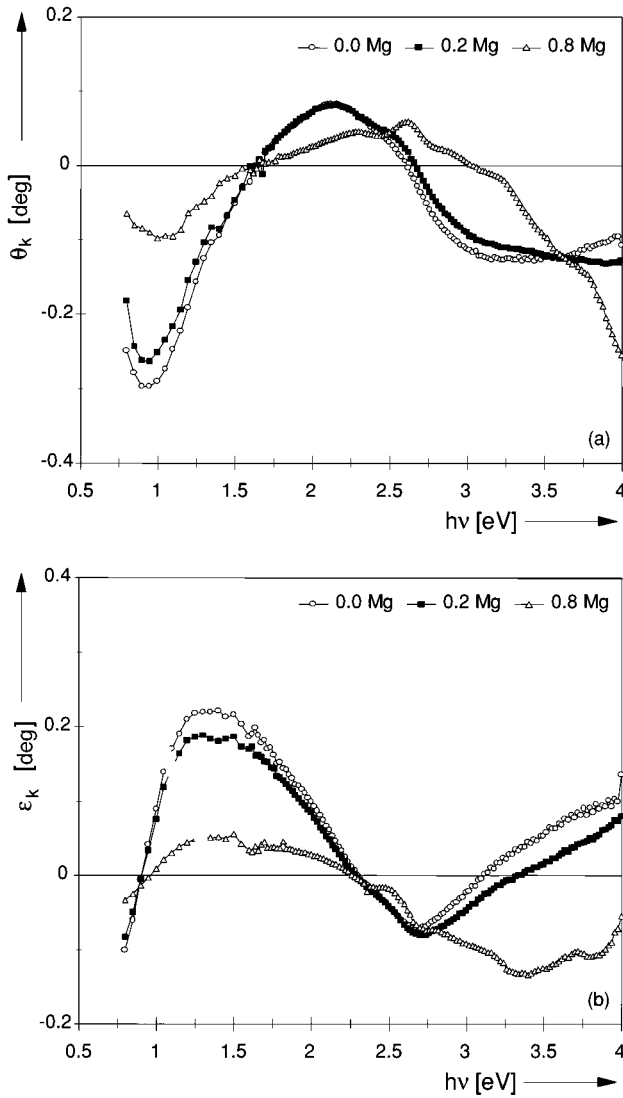
FIG. 5. The Kerr rotation θ_k (a) and Kerr ellipticity ϵ_k (b), of Mg-substituted Fe_3O_4: $(Fe^{3+})[Mg_x^{2+}Fe_{(1-x)}^{2+}Fe^{3+}]O_4$ for $x=0.0$, 0.2, and 0.8.

In Fig. 9 the influence of Al^{3+} substitution on the real and imaginary part of the off-diagonal element of the dielectric tensor is shown. In general, Al^{3+} mainly occupies B sites,[20] as in a normal spinel, where it replaces $[Fe^{3+}]$ and decreases the lattice parameter linearly down to 8.269 Å for $AlFe_2O_4$,[37,38] consistent with Vegard's law.[39] Due to its small ion radius, Al^{3+} will, more than Mg^{2+}, perturb the octahedral symmetry (and polarize O^{2-}).[25] The substitution of one octahedrally coordinated Fe^{3+} ion with Al^{3+} influences the electrostatic polarization and relative position of six oxygen anions. These oxygen anions are directly coupled to a total of six other B sites and six A sites. Thus, the substitution disturbs directly the trigonal symmetry of six tetrahedral clusters formed by three B sites and one A site with an oxygen anion at the center. Since each A site is part of four such clusters, another 18 tetrahedral clusters could be influenced. This would mean that for another 36 B sites the trigonal symmetry is lost. As a result, replacing 0.5% of the $[Fe^{3+}]$ would influence 10% of the octahedral sites. This is
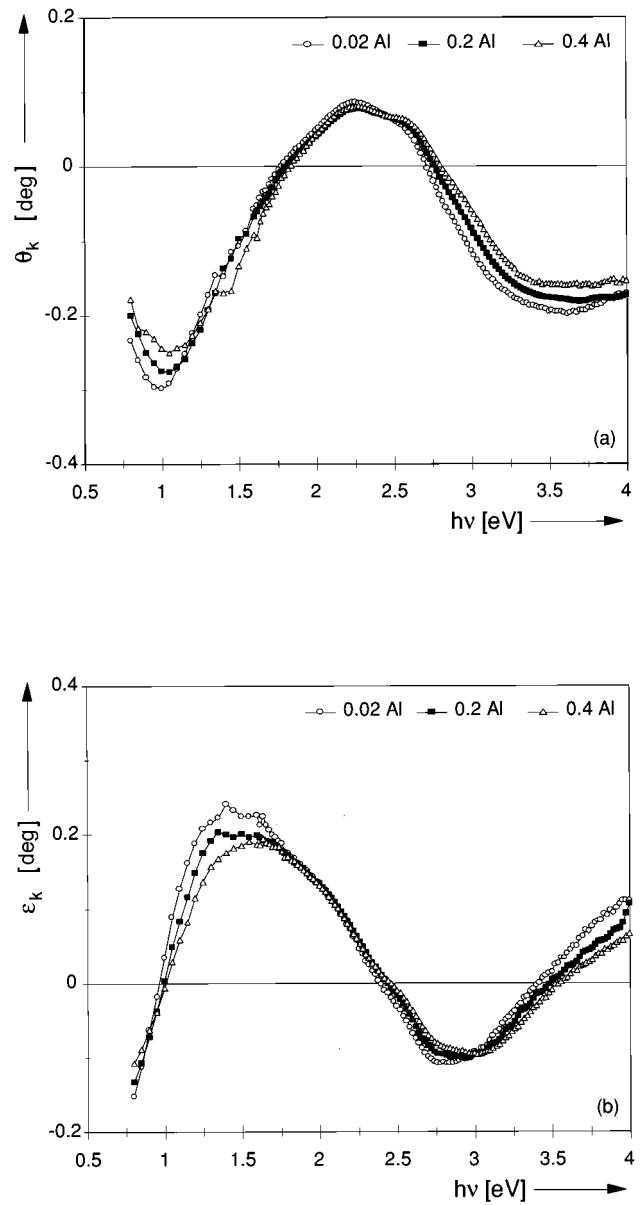
FIG. 6. The Kerr rotation θ_k (a) and Kerr ellipticity ϵ_k (b), of Al-substituted Fe_3O_4: $(Fe^{3+})[Al_x^{3+}Fe^{2+}Fe_{(1-x)}^{3+}]O_4$ for $x=0.02$, 0.2, and 0.4.

thought to be the cause of the pronounced effect on the MO spectrum of only a small amount of Al^{3+} (Fig. 9). Already a 0.005 Al^{3+} content (not shown) results in a shift of the total spectrum to higher energies, as well as an enhancement of the transitions around 0.56 and 3.0–4.0 eV. In Fig. 9(a) the extremum near 3 eV clearly shows a linear shift in energy and a decrease in ε_{xy}' upon Al^{3+} substitution.

So far, the observed effects of substitutions of Fe with the nonmagnetic Mg^{2+} and Al^{3+} on the off-diagonal element of the dielectric tensor: the comparatively small effect on the peak positions of Mg^{2+} substitution versus the comparatively large effect of Al^{3+} substitution and the pronounced effect of only a small amount of Al^{3+}, are not inconsistent with the proposition that IVCT transitions are at the basis of the MO spectrum of Fe_3O_4.
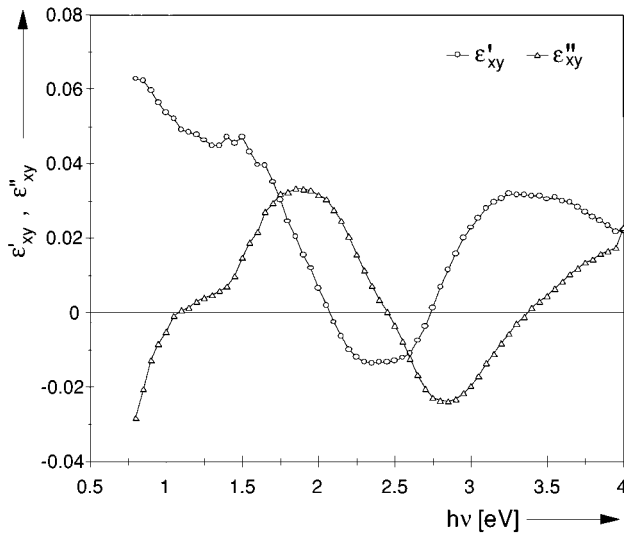
FIG. 7. The real (ε'_{xy}) and imaginary (ε''_{xy}) part of the off-diagonal element of the dielectric tensor of Fe_3O_4.

V. DATA-ANALYSIS AND DISCUSSION

A. Analysis of the spectra

To arrive at a correct transition assignment for Fe_3O_4, the exact peak positions in the substituted ferrites should also be determined. As we have seen above, peak positions in substituted ferrites may be shifted, in particular for Al^{3+}-substituted ferrites. In order to find the correct transition energies all spectra of the elements of the dielectric tensor were fitted by means of Eqs. (3) or (6) and (7). To evaluate the fits the three following criteria were used. First, the difference between the measured spectrum and the fit should be on average less than 1% of the tensor element. Secondly, one set of peaks should describe all four spectra, ε'_{xx}, ε''_{xx}, ε'_{xy}, and ε''_{xy} of a given ferrite. This fitting of *all four* elements of the dielectric tensor simultaneously is a more refined step in the analysis of the magneto-optical Kerr spectra of ferrites. Moreover, it is an essential step since due to the differences in line shape between the real and imaginary parts of the tensor elements overlapping bands can be resolved. Finally, the set of peaks should not depend on the Mg^{2+} or Al^{3+} substitution, as these ions are both nonmagnetic and the substitution is only partial. In Fig. 10 we show, by way of example, the fit to the imaginary part of (a) the diagonal element, ε''_{xx} and (b) the off-diagonal element, ε''_{xy}, of the dielectric tensor. The error in the fit is defined as the average difference between the fit and the dielectric tensor element in the energy range ± 0.1 eV from the transition energy. The importance of the third criterion can be illustrated by first considering the Fe_3O_4 spectra by themselves and only then taking the influence of Mg^{2+} substitution into account. All four Fe_3O_4 spectra can be described with a similar quality fit by a more limited set of transitions compared to the set reported in Table II. However, such a limited set of peaks fails to describe the spectra of Mg^{2+}-substituted ferrites. There are two reasons for this. First, a few strong transitions in the 3.0–4.0 eV range obscure other, weaker transitions. In Mg^{2+}-substituted ferrites strong Fe^{2+}-dependent transitions are suppressed, allowing the detection of weaker Fe^{3+}-dependent peaks. Second, a complicating factor is that
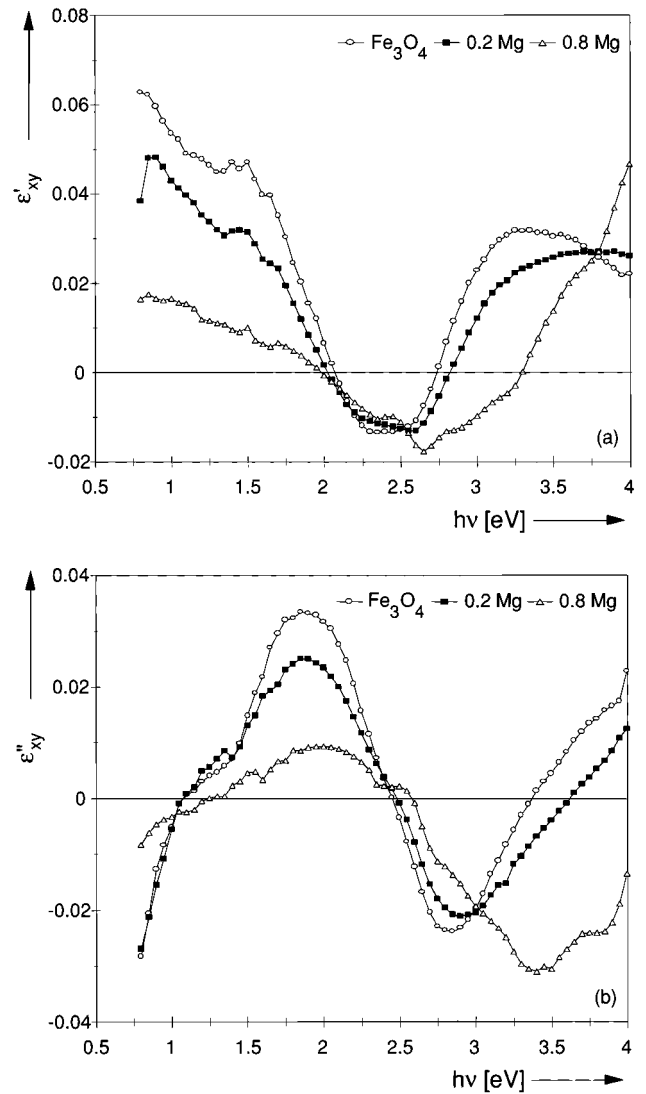
FIG. 8. The off-diagonal element of the dielectric tensor of $(Fe^{3+})[Mg_x^{2+}Fe_{(1-x)}^{2+}Fe^{3+}]O_4$ for $x = 0.0$, 0.2, and 0.8; (a) real part, ε'_{xy}; (b) imaginary part, ε''_{xy}.

around 4.0 eV two relatively strong transitions with identical line shapes but opposing signs are present.

Thus by means of the Mg^{2+} substitution the Fe_3O_4 spectrum could be unravelled. In addition, we could determine which transitions are dependent on Fe^{2+} content, and which are not. This leads to the more complete set of transitions given in Table II, which describes all spectra throughout the range of Mg^{2+} and Al^{3+} substitution.

B. Peak assignment and discussion

The key results that enable us to assign of the main transitions are given in Fig. 11. In Fig. 11(a) the maximum ε_{xy} value is given, relative to the value for Fe_3O_4, versus $[Fe^{2+}]$ content of the Mg^{2+}-substituted ferrite, for the transitions at 0.56, 1.94, 3.11, and 3.93 eV. Similarly Fig. 11(b) gives the relative maximum ε_{xy} value versus $[Fe^{3+}]$ content of the Al^{3+}-substituted ferrite for the same transitions. Substitution with Mg^{2+} [Fig. 11(a)] as well as substitution with Al^{3+} [Fig. 11(b)] causes a marked decrease in ε''_{xy} for the transi-
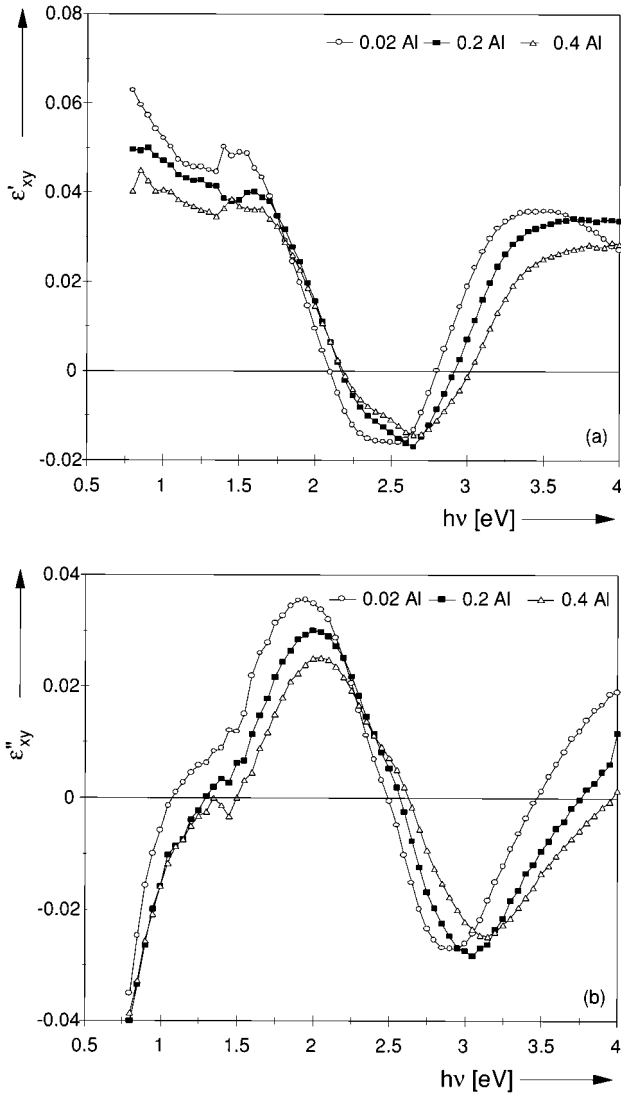
FIG. 9. The off-diagonal element of the dielectric tensor of $(Fe^{3+})[Al_x^{3+}Fe^{2+}Fe_{(1-x)}^{3+}]O_4$ for $x = 0.02$, 0.2, and 0.4; (a) real part, ε'_{xy}; (b) imaginary part, ε''_{xy}.

FIG. 10. The fit to the imaginary part of (a) the diagonal element, ε''_{xx}, and (b) the off-diagonal element, ε''_{xy}, of the dielectric tensor, for Fe_3O_4.

tion at 0.56 eV.[40] Hence, for this transition both $[Fe^{2+}]$ and $[Fe^{3+}]$ are involved. Therefore, the transition at 0.56 eV is assigned to intervalence charge transfer (IVCT): $[d^5] + [d^6] \rightarrow [d^6] + [d^5]$ at B sites. More specifically, it is the lowest IVCT $t_{2g} \rightarrow t_{2g}$ (see Fig. 12) in accordance with the proposition of Feil.[7]

Assignment of the band at 1.94 eV is more complex because several transitions, including weak crystal-field transitions,[10,11] overlap here. The main transition, however, is IVCT: $t_{2g} \rightarrow e_g$ between $[Fe^{2+}]$ and $[Fe^{3+}]$. This is the next IVCT (see Fig. 12). As can be seen in Fig. 11(a), substitution with Mg^{2+} again exerts a clear influence. In addition, Fig. 11(b) shows that Al^{3+} substitution has the same effect as on the transition at 0.56 eV. Hence, for this transition again both $[Fe^{2+}]$ and $[Fe^{3+}]$ are involved.

The transition at 3.11 eV is assigned to IVCT transition: $t_{2g} \rightarrow e$, i.e., from $[Fe^{2+}]$ to (Fe^{3+}). Note the notation for A-site and B-site ions which are between parentheses and square brackets, respectively. Again we observe a dependence on Mg^{2+} substitution [Fig. 11(a)]. However, in this

case Al^{3+} substitution [Fig. 11(b)] has no significant effect on the intensity of the transition after the initial change on substitution of Fe^{3+} with 0.02 Al^{3+}. Finally, the transition at 3.93 eV is assigned to the IVCT transition $t_{2g} \rightarrow t_2$, which exhibits similar behavior upon Mg^{2+} and Al^{3+} substitution as the transition at 3.11 eV does (Fig. 11).

Next, we consider the line shapes of these transitions, reported in Table II. For the transition at 0.56 eV, $[Fe^{2+}]t_{2g} \rightarrow [Fe^{2+}]t_{2g}$, both the ground state and the excited state are split. In addition there is a distinct difference in occupation of the t_{2g} ground state levels (see Fig. 12). Furthermore, the band-structure calculations by Feil show that the t_{2g} band in Fe_3O_4 is relatively broad.[7] This will mask the effect of the split excited state and as a result the shape of the transition will be determined by the difference in ground-state populations, i.e., the difference in oscillator strength for $\Delta m_l = 1$ (RCP) and $\Delta m_l = -1$ (LCP). Hence, the observed paramagnetic line shape is expected. In the case of the transition at 1.94 eV, $[Fe^{2+}]t_{2g} \rightarrow [Fe^{2+}]e_g$, only the partially occupied ground state is split and the aforementioned band-

TABLE II. The main transitions occurring in Fe_3O_4 between 0.5 and 5.0 eV. Listed are peak position ω_0, width Γ_0, intensity $(\varepsilon_{xy})_{max}$, as well as peak assignment. For details see text.

ω_0 (eV)	Γ_0 (eV)	$(\varepsilon_{xy})_{max}$	Type	Transition	Shape
			Strongly dependent on Fe^{2+}		
0.56	0.21	-0.085	IVCT	$[Fe^{2+}]t_{2g} \rightarrow [Fe^{2+}]t_{2g}$	$-$para
1.94	0.45	0.044	IVCT	$[Fe^{2+}]t_{2g} \rightarrow [Fe^{2+}]e_g$	$+$para
3.11	0.61	0.031	IVCT	$[Fe^{2+}]t_{2g} \rightarrow (Fe^{2+})e$	$+$dia
3.93	0.37	-0.039	IVCT	$[Fe^{2+}]t_{2g} \rightarrow (Fe^{2+})t_2$	$-$dia
			Weakly dependent on Fe^{2+}		
2.61	0.20	-0.004	ISCT	$(Fe^{3+})t_2 \rightarrow [Fe^{2+}]t_{2g}$	$-$dia
			(ISCT)	$([Fe^{3+}]e_g \rightarrow (Fe^{2+})e)$	
3.46	0.42	0.014	ISCT	$[Fe^{3+}]e_g \rightarrow (Fe^{2+})t_2$	$+$dia
3.94	0.51	0.065	ISCT	$(Fe^{3+})t_2 \rightarrow [Fe^{2+}]e_g$	$+$dia
4.51	0.40			$(O_{2p} \rightarrow [Fe^{2+}])$	

structure calculation shows that the e_g band is also relatively broad, hence a paramagnetic line shape is again observed for this transition. The band-structure calculations further show that the bands situated on the tetrahedral sublattice are distinctly narrower than the bands on the octahedral sublattice.
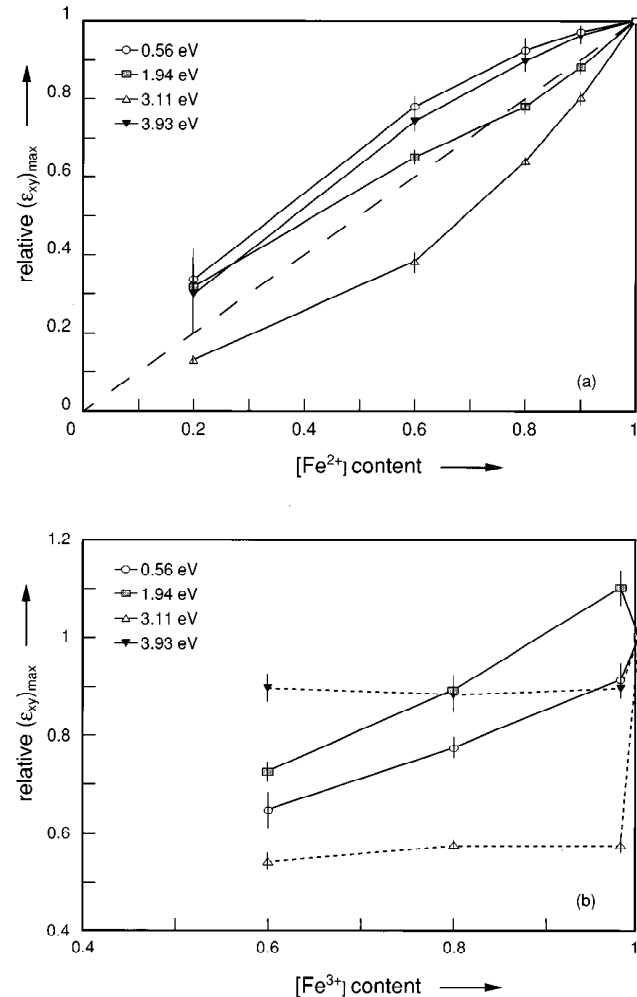
FIG. 11. Relative maximum ε_{xy} value for the IVCT transitions; (a) versus $[Fe^{2+}]$ content (Mg substitution), (b) versus $[Fe^{3+}]$ content (Al substitution).

As a result we observe a diamagnetic line shape for the transitions at 3.11 and 3.93 eV, $[Fe^{2+}]t_{2g} \rightarrow (Fe^{2+})e$ and $[Fe^{2+}]t_{2g} \rightarrow (Fe^{2+})t_2$, respectively, since the difference in energy between the transitions with selection rules $\Delta m_l = 1$ and $\Delta m_l = -1$ will determine the line shape.

Regarding the relative strength of the IVCT transitions, we observe (Table II) that transitions between two t orbitals are stronger than transitions between a t and an e orbital and that the transitions between cations on the octahedral sublattice are stronger than the transitions between the two sublattices. Both effects are to be expected. First, $t_{2g} - t_{2g}$ orbitals have a large overlap, as these orbitals point towards each other in between the oxygen anions. The $t_{2g} - e_g$ orbitals have a much smaller overlap as the e_g is directed towards the oxygen anion.[7,41] Secondly, as electron spin reorientation upon excitation is an improbable process, transitions between antiferromagnetically coupled ions are weaker than between ferromagnetically coupled ions. A theoretical analysis has, however, shown that IVCT transitions between antiferromagnetically coupled ions are still possible, albeit at reduced intensity.[29]

The data in Fig. 11(a) show that the MO transitions depend in a nonlinear manner on the $[Fe^{2+}]$ concentration. Within the margin of error no straight line can be drawn through the datapoints. This can be seen by comparing these points with the straight dotted line in Fig. 11(a) representing a linear dependence. According to some authors this already
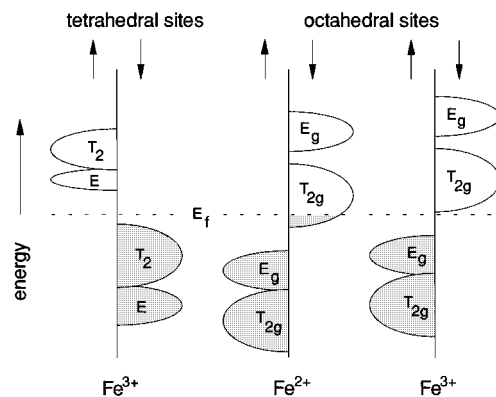
FIG. 12. Schematic representation of the electronic structure of the Fe ions in Fe_3O_4.

indicates that a pair interaction is responsible for this transition.[7,42] The argument is that normally the oscillator strength of a transition is independent of the concentration of the absorbing species. This results in a linear dependence of the intensity of a transition on the concentration in the case of a single-ion transition (Lambert-Beer law).[18,23,24] If the absorption process involves pairs of ions, as in the case of an IVCT or ISCT transition, the Lambert-Beer law no longer applies and a nonlinear dependence on the concentration may be observed.[7,42] In ferrites this simple situation may be complicated by disturbances of the lattice upon substitution. However, in the case of substitution with Mg^{2+} the lattice parameter changes less than 0.3% in the case of complete substitution of Fe^{2+}.[1] As a result the lattice is hardly disturbed. In contrast, the delocalization α is expected to be influenced by Mg substitution as the electron is now pinned on the Mg^{2+} site. Hence, referring to Eq. (9), a nonlinear dependence of $(\varepsilon_{xy})_{max}$ on Mg^{2+} substitution can be expected for IVCT transitions.

The transitions that are only weakly dependent on Fe^{2+} content are reported in the second part of Table II. The transitions in the 2.5–4.0 eV range have the same relative position, linewidth, and relative intensity as the ISCT transitions reported by Scott[18] for yttrium iron garnet (YIG). Hence, we attribute these transitions to intersublattice charge transfer transitions. Since in this case for the ground state the split t orbitals are fully occupied while the ground-state e orbitals are not split, we expect the observed diamagnetic line shape for all ISCT transitions. The transition at 4.51 eV was assigned by Scott to the first O $2p \rightarrow$ Fe $3d$ charge-transfer transition. We have been unable to draw any conclusion concerning this assignment, as no MO data were available above 4.0 eV.

As a final check on the consistency of the peak assignment given in Table II, the relative energy differences of the excited states can be calculated. From the foregoing it follows that the difference between the energies of the first two IVCT transitions (1.38 eV) must be equal to the difference between the first and the last ISCT transition (1.33 eV) as both these differences reflect the crystal-field splitting between t_{2g} and e_g. The values thus obtained are in fair agreement with the crystal-field splitting between t_{2g} and e_g calculated by Feil (1.5 eV) (Ref. 7) and derived by Camphausen, Coey, and Chakraverty (1.3 eV).[3] Furthermore, the difference between the energies of the last two IVCT transitions (0.82 eV) should equal the difference between the

middle ISCT transition and the ISCT transition: $[Fe^{3+}]e_g \rightarrow (Fe^{2+})e$. This last transition should then be situated around 2.64 eV and can therefore, unfortunately, not be separated from the $(Fe^{3+})t_2 \rightarrow [Fe^{2+}]t_{2g}$ transition at 2.61 eV which has the same line shape. In addition, in YIG the latter transition is reported to be about twice as intense as the former.[18] The crystal-field splitting between t_2 and e is calculated by Feil to be 1 eV (Ref. 7) and derived by Camphausen, Coey, and Chakraverty to be 0.8 eV.[3]

VI. CONCLUSIONS

We have measured both the optical and the magneto-optical polar Kerr spectrum of pure Fe_3O_4 and of Mg^{2+}-substituted and Al^{3+}-substituted Fe_3O_4 at 293 K. This has enabled us to determine the complete dielectric tensor of these compounds between 0.7 and 4.0 eV. Key to the subsequent unravelling of the complicated Fe_3O_4 spectra were the following: First the fitting of all four (ε'_{xx}, ε''_{xx}, ε'_{xy}, and ε''_{xy}) parts of the dielectric tensor *simultaneously* with one set of transitions. As a result overlapping bands can be resolved due to the differences in line shape between the real and imaginary parts of the tensor elements. Second, the systematic substitution with nonmagnetic ions, of which the Mg^{2+} substitution was essential to separate the intense, Fe^{2+}-dependent IVCT transitions from the ISCT transitions. The observed dependence on both $[Mg^{2+}]$ and $[Al^{3+}]$ of certain MO transitions have provided us with experimental evidence that IVCT transitions are at the basis of the Fe_3O_4 MO-Kerr spectrum. The assignment of the main MO active transitions in Fe_3O_4 to IVCT transitions is consistent with the observed line shapes, relative strengths, and relative transition energies. Furthermore, ISCT transitions consistent with YIG could be identified. The IVCT transitions occur at 0.56, 1.94, 3.11, and 3.94 eV. From these transitions we find, in agreement with the assignment of the ISCT transitions, that in Fe_3O_4 the $t_{2g} - e_g$ excited state energy or crystal-field splitting of octahedral Fe^{3+} is 1.38 eV and that the $t_2 - e$ energy splitting of tetrahedral Fe^{3+} is 0.82 eV.

ACKNOWLEDGMENTS

*Author to whom correspondence should be addressed.

[1] J. Smit and H. P. J. Wijn, *Ferrites* (Philips Technical Library, Eindhoven, 1959).

[2] V. A. M. Brabers, in *Handbook of Magnetic Materials*, edited by K. H. J. Buschow (Elsevier Science, Amsterdam, 1995), Vol. 8, p. 199.

[3] D. L. Camphausen, J. M. D. Coey, and B. K. Chakraverty, Phys. Rev. Lett. **29**, 657 (1972).

[4] Y. Yanasa and K. Siratori, J. Phys. Soc. Jpn. **53**, 312 (1984).

[5] J. Zaanen, G. A. Sawatzky, and J. W. Allen, Phys. Rev. Lett. **55**, 418 (1985).

[6] R. A. de Groot and K. H. J. Buschow, J. Magn. Magn. Mater. **54-57**, 1377 (1986).

[7] H. Feil, Ph.D. thesis, University of Groningen, Groningen, The Netherlands, 1987; Solid State Commun. **69**, 245 (1989).

[8] J. Zaanen and G. A. Sawatzky, J. Solid State Chem. **88**, 8 (1990).

[9] Z. Zhang and S. Sapathy, Phys. Rev. B **44**, 13 319 (1991).

[10] Z. Šimša, H. LeGall, and P. Siroky, Phys. Status Solidi B **100**, 665 (1980).

[11] Z. Šimša, P. Široký, J. Koláček, and V. A. M. Brabers, J. Magn. Magn. Mater. **15-18**, 775 (1980).

[12] X. Zhang, J. Schoenes, and P. Wachter, Solid State Commun. **39**, 189 (1981).

[13] X. Zhang, J. Schoenes, W. Reim, and P. Wachter, J. Phys. C **16**, 6055 (1983).

[14] Š. Višňovský, V. Prosser, R. Krishnan, V. Pařízek, K. Nitsch, and

L. Svobodová, IEEE Trans. Magn. **MAG-17**, 3205 (1981).

[15] W. L. Peeters and J. W. D. Martens, J. Appl. Phys. **53**, 8178 (1982).

[16] J. L. Erskine and E. A. Stern, Phys. Rev. B **8**, 1239 (1973).

[17] L. Degiorgi, I. Blatter-Mörke, and P. Wachter, Phys. Rev. B **35**, 5421 (1987); L. Degiorgi, P. Wachter, and D. Ihle, *ibid.* **35**, 9259 (1987).

[18] G. B. Scott, in *Physics of Magnetic Garnets*, edited by A. Paoletti (Societa Italiana di Fisica, Bologna, 1978).

[19] V. A. M. Brabers and J. Klerk, J. Phys. (France) Colloq. **38**, C1-207 (1977).

[20] M. Rosenberg, P. Deppe, H. H. Janssen, V. A. M. Brabers, F. S. Li, and S. Dey, J. Appl. Phys. **57**, 3740 (1985).

[21] W. Reim and J. Schoenes, in *Handbook of Ferromagnetic Materials*, edited by E. P. Wohlfarth and K. H. J. Buschow (North-Holland, Amsterdam, 1990).

[22] F. J. Kahn, P. S. Pershan, and J. P. Remeika, Phys. Rev. **186**, 891 (1969).

[23] S. Wittekoek, T. A. J. Popma, J. M. Robertson, and P. F. Bongers, Phys. Rev. B **12**, 2777 (1975).

[24] G. B. Scott, D. E. Lacklison, H. I. Ralph, and J. L. Page, Phys. Rev. B **12**, 2562 (1975).

[25] G. C. Allen and N. S. Hush, in *Progress in Inorganic Chemistry*, edited by F. A. Cotton (Interscience, New York, 1967).

[26] M. B. Robin and P. Day, in *Advances in Inorganic Chemistry and Radiochemistry*, edited by H. J. Emeléus and A. G. Sharpe (Academic, New York, 1967).

[27] D. M. Sherman, Phys. Chem. Miner. **14**, 355 (1987).

[28] D. M. Sherman, Phys. Chem. Miner. **12**, 161 (1985).

[29] P. A. Cox, Chem. Phys. Lett. **69**, 340 (1980).

[30] See, for instance, P. J. van der Zaag, A. Noordermeer, M. T. Johnson, and P. F. Bongers, Phys. Rev. Lett. **68**, 3112 (1992), and references therein; V. A. M. Brabers, *ibid.* **68**, 3113 (1992), and references therein.

[31] V. A. M. Brabers, T. E. Whall, and P. S. A. Knapen, J. Cryst. Growth **69**, 101 (1984).

[32] J. W. D. Martens, W. L. Peeters, P. Q. J. Nederpel, and M. Erman, J. Appl. Phys. **55**, 1100 (1984).

[33] K. Sato, Jpn. J. Appl. Phys. **20**, 2403 (1981).

[34] W. B. Zeper, Ph.D. thesis, University of Twente, Enschede, The Netherlands, 1991.

[35] P. A. M. van der Heide, Ph.D. thesis, University of Nijmegen, The Netherlands, 1985; J. C. Jans, Philips J. Res. **47**, 347 (1993).

[36] I. Müller and U. Buchenau, Physica B & C **80B**, 69 (1975).

[37] L. de Bont and V. A. M. Brabers (unpublished).

[38] A. Petric, K. T. Jacob, and C. B. Alcock, J. Am. Ceram. Soc. **64**, 632 (1981).

[39] A. E. West, *Solid State Chemistry and its Applications* (Wiley, Chichester, 1984).

[40] Note that the ε_{xx} spectra have been determined between 0.5 and 5.0 eV. Consequently, although the 0.56 eV transition is beyond the range where MO measurements have been made the peak position is well established from the optical data. Furthermore, the 0.56 eV peak position is consistent with previous experiments (Refs. 7, 10, and 13). Moreover, this transition is relatively strong, which allows an unambiguous determination of line shape and transition energy.

[41] G. B. Scott and J. L. Page, Phys. Status Solidi B **79**, 203 (1977).

[42] G. B. Scott and D. E. Lacklison, IEEE Trans. Magn. **MAG-12**, 292 (1976).